J Ther Eng, Vol. 8, No. 4, pp. 477–489, July 2022

Journal of Thermal Engineering
Web page info: https://jten.yildiz.edu.tr
DOI: 10.18186/thermal.1145424

Journal of Thermal Engineering

Research Article

Performance improvement methods for quartz tube solid particle fluidized bed solar receiver

Mehmet BÖLÜK[1], Senem ŞENTÜRK LÜLE[1,*]

[1]*Energy Institute, İstanbul Technical University, Istanbul, Türkiye*

ARTICLE INFO

Article history
Received: 30 December 2021
Accepted: 19 March 2022

Keywords:
Computational Fluid Dynamics; Concentrated Solar System; Solid Particle Receiver; Two Phase Flow

ABSTRACT

The conditions to improve performance of quartz tube silicon carbide (SiC) solid particle fluidized bed solar receiver was investigated with computational fluid dynamics (CFD) simulations. The difficulty of experimenting all possible operating conditions was overcome by preparing CFD base input with appropriate models and parameters. The amount of SiC in the bed, the size of particles, and the air inlet velocity were considered as variables. After model verification, in order to evaluate the effect of particle addition, bed without solid particles were simulated first. Outlet temperature of single-phase receiver was calculated as 421 K. Outlet temperatures of 913 K, 895 K, and 881 K were obtained for 400 μm diameter particles in 0.3 m bed height for air inlet velocities of 0.25, 0.3, and 0.35 m/s. Air outlet temperature decreases as air inlet velocity increases. On the other hand, too much reduction at inlet velocity retards the system performance since it affects fluidization. For 400 μm particle diameter and bed height of 0.2 m, outlet temperatures of 994 K, 974 K, and 955 K were found for the same air inlet velocities above. As bed height decreases, air outlet temperature increases. For particle diameters of 300 and 500 μm for bed height of 0.3 m, outlet temperatures of 980 K and 878 K were calculated for appropriate minimum fluidization velocities. Outlet temperature increased with decreasing particle size.

Cite this article as: Bölük M, Şentürk Lüle S. Performance improvement methods for quartz tube solid particle fluidized bed solar receiver. J Ther Eng 2022;8(4):477–489.

INTRODUCTION

Since the large-scale use of fossil fuels produces many harmful substances and greenhouse gases for the environment, technologies without carbon emission becomes vital instruments in meeting energy needs. Along with nuclear energy, solar and wind energies are good options for such an important trend. Generating electricity by radiation from the sun can be divided into two main categories: photovoltaic (PV) and concentrated solar energy (CSE) systems. In photovoltaic systems, solar radiation is absorbed with the help of solar panels and electricity is produced. In

***Corresponding author.**
*E-mail address: senturklule@itu.edu.tr

This paper was recommended for publication in revised form by Regional Editor Emre Alpman

Published by Yıldız Technical University Press, İstanbul, Turkey

concentrated solar energy systems, the solar radiation is absorbed in a heat carrier environment and then electricity is produced by using this carrier. In the last few years, there has been serious increase in the number of photovoltaic systems due to the rapid decrease in panel production costs and the increase in panel efficiency. However, concentrated solar energy systems offer advantages such as thermal storage and combination ability with other energy systems. In contrast, photovoltaic systems also offer storage options using electrochemical batteries. However, the technology is not yet as cheap as one would like.

By adding solid particles into the receivers in CSE systems, system outlet temperatures higher than 1000 °C can be achieved due to direct or indirect exposure of these particles to concentrated solar radiation [1]. With these high temperatures, high efficiency can be accomplished in supercritical Carbon Dioxide (CO_2) Brayton cycle or ultra-supercritical vapor conversion systems. Solid particle receivers provide advantages like increase in heat transfer rate, process stability, low particle loss, and easy control of gas flow rate.

In recent years, many research institutions have developed solar receiver models and carried out experiments [2]. Researchers from the Sandia National Laboratory (SNL) working on direct radiation solid particle solar receivers (SPSR) conducted two series of tests related with the area of exposure to solar radiation, in free-falling SPSR systems in 2008 and 2016 [3]. Reducing the designed opening area from 4.5 m^2 to 1 m^2 greatly reduced the convective heat loss and increased the thermal efficiency from 33-53% to 50-80%.

In addition, in subsequent experiments, the particles were recirculated in the system so that the solid particles were more exposed to solar radiation, allowing the particle outlet temperature to exceed 700 °C. In order to prolong the residence time of the particles in the system, Kim et al. (2019) [4] proposed a multi-stage free-falling SPSR system and obtained stable particle curtain in cold flow tests with a drop height of 5 meters. Placing barriers in the flow channel was considered as an alternative solution to increase the particle temperature per unit length. Ho et al. (2016) [5] performed tests with grating curtains under a radiation intensity of 300-400 kW/m^2 and obtained an average temperature of 150-200 °C/m and a thermal efficiency of 90%. However, SS316 stainless steel grates were found to be destroyed after 20 hours of heating cycles. By using low-cost desert sand, a thermal efficiency of 60-70% was obtained in steel grating systems in Saudi Arabia [6].

Particle loss is a common disadvantage in direct radiation SPSR systems [5] that causes various indirect radiation SPSR systems to be proposed. In this context, Lopez et al. (2016) [7] performed a test using a fluidized bed solar receiver. In this test, solid particles were used in 16 upstream tubes, and thermal efficiency of 52-90% and average temperature of 137-335 °C/m were obtained at a radiation intensity of 63-142 kW/m^2 and a mass flux of 17-44 kg/m^2-s. Benoit et al. [8] tested the particle-wall heat transfer coefficient in a metal tube fluidized bed receiver and found that the results ranged from 400-1000 W/m^2-K. Johnson et al. (2016) [9] presented a particle-filled receiver model with particles flowing down in a vertical steel tube. Preliminary trials were carried out with a 12 m copper pipe wrapped with electrical heating elements. However, the average temperature rise was only 33-125 °C/m at a mass flux of 54.6-257 kg/m^2-s. A system in which particles flow down through the helical quartz tube was first developed and tested by the Chinese Academy of Sciences in 2017. When the particle mass flow rate was 8.12 g/s and the direct radiation intensity was 500 W/m^2, temperature increase of 212 °C and thermal efficiency of 61.2% were obtained at the 0.2 m radiation aperture [10]. Thanks to the length of the helical quartz tube radiation aperture section, the residence time of the particles in the radiation area increased providing an advantage over other systems. As an alternative to this design, gravity-operated moving bed solid particle solar receiver has been developed by Nie et al. (2019) [11], providing a stable particle flow with a reasonable particle layer thickness and average particle size.

In parallel with these studies, the Electrical Engineering Institute of the Chinese Academy of Sciences (CAS) designed a quartz glass tube solid particle air receiver and carried out experimental and numerical simulation studies [12]. In this receiver, the air flow enters the receiver through a fan, forming a bottom-up flow together with the silicon carbide (SiC) particles with an average size of 5 mm, so that the solid particles directly absorb the solar radiation. Experimental results showed that the outlet temperature of the air could exceed 600 °C and the temperature difference between solid and air could be less than 25 °C. In 2001, Segal and Epstein [13] pioneered the idea of replacing the solar tower with a secondary condensing system to reduce the cost of the power plant and energy loss during transportation. Based on this concept, Kodama et al. (2016) [14] proposed a fluidized bed particle receiver. In this receiver, a system that injects high velocity air into the central ring and low velocity air into the outer ring was used to fluidize the particles. The receiver is equipped with a guide plate to regulate the particle circulation and a transparent quartz glass window on top. Solar radiation from above heats the fluidized particles inside. Kodama et al. (2017) [15] showed that under 100 kW_{th} power, the solid particle temperature and outlet temperature in the receiver center can reach 960-1100 °C and 1100 °C, respectively. In many cases though, fluidized bed solar receiver with a transparent solar window is accepted as a direct radiation SPSR [16].

In addition to experimental studies, numerical methods were also used to examine the flow and heat transfer processes inside the SPSR receiver. Bellan et al. (2019) [17] combined the 3D heat and mass transfer model with computational fluid dynamics and investigated the bubble formation, coalescence and dissociation in the receiver with

simulations. Briongos et al. (2019) [18] simulated the flow and heat transfer processes of fluidized bed solid particle air receivers based on a secondary condensation system using the Euler-Euler model and investigated the effect of operating parameters on performance.

In this study, performance improvement methods for quartz tube solid particle fluidized bed solar receiver with upward flow defined by Wang et al. (2016) [10] was examined with ANSYS Fluent computational fluid dynamics (CFD) software. Therefore, the challenge of performing experiments for all possible operating conditions was overcome. Although, CFD simulations are excellent tools for simulating physics, it is important to select appropriate models and parameters in the software. For this purpose, benchmarking with experimental data was performed. In order to analyze performance improvement methods, the air inlet velocity, the bed height, and particle size were selected as variable parameters.

MATHEMATICAL MODEL

Two-phase flow modeling was used as the solid and fluid phases were simultaneously present in the receiver. Although different methods, such as the Volume of Fluid Model (if system has two or more immiscible fluids) and Mixture Model (if system has two or more phases and the solid loading is below 10%), can be used to simulate two-phase flow with CFD, the Euler-Euler method (applicable for granular and non-granular flows) was chosen in this study since the volume fraction of solid phase in the fluidized bed system investigated in this study is over 10% [19].

Since all phases in the system are considered continuous in Euler-Euler method, each phase is expressed by the "phase volume fraction α" shown in Equation 1 [20]. The sum of the phase volume fractions in the system for all phases is equal to one as shown in Equation 2 [20].

$$V_q = \int_V \alpha_q dV \tag{1}$$

$$\sum_{q=1}^{n} \alpha_q = 1 \tag{2}$$

where, V_q is the volume of the phase q and n is the number of phases. Since there are two phases, solid and gas, in this study, the solid phase is expressed with the subscript p and gas phase is expressed with the subscript f. In this case, for this study, the equation $\alpha_p + \alpha_f = 1$ exists.

The continuity, momentum, and energy equations solved for the two continuous phases are listed between Equation 3 and Equation 8 [21].

The Equations of the Gas Phase

Continuity Equation:

$$\frac{\partial}{\partial t}\left(\alpha_f \rho_f\right) + \nabla.\left(\alpha_f \rho_f \vec{u}_f\right) = 0 \tag{3}$$

where, α_f is the air volume fraction, ρ_f is the air density, and $\vec{u}_f$ is the air velocity.

Momentum Equation:

$$\frac{\partial}{\partial t}\left(\alpha_f \rho_f \vec{u}_f\right) + \nabla.\left(\alpha_f \rho_f \vec{u}_f \vec{u}_f\right) = -\alpha_f \nabla p + \nabla.\bar{\bar{\tau}}_f + \alpha_f \rho_f \vec{g} + \sum_{i=1}^{n}\left(\vec{R}_{if}\right) + \left(\vec{F}_f + \vec{F}_{l,f} + \vec{F}_{wl,f} + \vec{F}_{vm,f}\right) \tag{4}$$

where, p is the pressure shared by the all phases, $\bar{\bar{\tau}}_f$ is the Reynolds stress tensor of air, $\vec{g}$ is the gravitational acceleration, $\vec{R}_{if}$ is interaction force between the solid and the gas phase, $\vec{F}_f$ is external body force, $\vec{F}_{l,f}$ is the lift force, $\vec{F}_{wl,f}$ is a wall lubrication force, and $\vec{F}_{vm,f}$ is the virtual mass force.

Energy equation:

$$\frac{\partial}{\partial t}\left(\alpha_f \rho_f h_f\right) + \nabla.\left(\alpha_f \rho_f \vec{u}_f h_f\right) = \alpha_f \frac{\partial p_f}{\partial t} + \bar{\bar{\tau}}_f : \nabla \vec{u}_f - \nabla.\vec{q}_f + S_f + \sum_{i=1}^{n} Q_{fi} \tag{5}$$

where h_f is the specific enthalpy of the air phase, p_f is the pressure of the air, $\vec{q}_f$ is the heat flux, S_f is a source term that includes of enthalpy, and Q_{fi} is the intensity of heat exchange between phases.

The Equations of Solid Phase

Continuity Equation:

$$\frac{\partial}{\partial t}\left(\alpha_p \rho_p\right) + \nabla.\left(\alpha_p \rho_p \vec{u}_p\right) = 0 \tag{6}$$

Momentum Equation:

$$\frac{\partial}{\partial t}\left(\alpha_p \rho_p \vec{u}_p\right) + \nabla.\left(\alpha_p \rho_p \vec{u}_p \vec{u}_p\right) = -\alpha_p \nabla p + \nabla.\bar{\bar{\tau}}_p + \alpha_p \rho_p \vec{g} + \sum_{i=1}^{n}\left(\vec{R}_{ip}\right) + \left(\vec{F}_p + \vec{F}_{l,p} + \vec{F}_{wl,p} + \vec{F}_{vm,p}\right) \tag{7}$$

Energy Equation:

$$\frac{\partial}{\partial t}\left(\alpha_p \rho_p h_p\right) + \nabla.\left(\alpha_p \rho_p \vec{u}_p h_p\right) = \alpha_p \frac{\partial p_p}{\partial t} + \bar{\bar{\tau}}_p : \nabla \vec{u}_p - \nabla.\vec{q}_p + S_p + \sum_{i=1}^{n} Q_{pi} \tag{8}$$

Since solid particles in the SPSR system play an important role in the absorption and scattering of solar radiation, among possible options in Fluent software, the Discrete Ordinates Radiation Model was adopted. This model spans the entire range of optical thicknesses, allows usage from surface-to-surface radiation to participating radiation in

combustion problems, and allows the solution of radiation at semi-transparent walls. In this model, the radiation transfer equation is solved for a finite number of discrete solid angles, each associated with a vector direction $\vec{s}$ fixed in the global Cartesian system. The discrete coordinates radiation model assumes the radiation transfer equation in the $\vec{s}$ direction as a field equation.

$$\nabla\left(\mathrm{I}(\vec{r},\vec{s})\vec{s}\right)+\left(\alpha\sigma_s\right)\mathrm{I}(\vec{r},\vec{s})= \alpha\omega^2\frac{\sigma.T^4}{\pi}+\frac{\sigma_s}{4\pi}\int_0^{4\pi}\mathrm{I}\left(\vec{r},\vec{s}^{\,`}\right)\phi\left(\vec{s},\vec{s}^{\,`}\right)d\Omega' \quad (9)$$

In Equation 9, I is the radiation intensity, $\vec{r}$ the position vector, $\vec{s}$ the direction vector, α the absorption coefficient, σ_s the scattering coefficient, ω the refractive index, σ the Stefan Boltzmann constant, ϕ the phase density, $\vec{s}'$ the scattering direction vector, and Ω' the represents the solid angle.

In order to calculate the heat transfer between solid particles and air, the Gunn model (Equation 10 [22]), which uses kinetic theory of granular flows and is frequently used in the Euler-Euler model simulations of two-phase flows containing dense solid phase which is the case in this study, was preferred for the calculation of Nusselt number Nu_{fp}.

$$Nu_{fp}=\left(7-10\alpha_f+5\alpha_f^{\,2}\right)\left(1+0.7Re^{0.2}Pr^{1/3}\right)+ \left(1.33-2.4\alpha_f+1.2\alpha_f^{\,2}\right)Re^{0,7}Pr^{1/3} \quad (10)$$

where Re is Reynolds number (Equation 11 [23]), and Pr is Prandtl number (Equation 12 [23]).

$$Re=\left|u_f-u_p\right|d_p\rho_f/\mu_f \quad (11)$$

$$Pr=c_{pf}\mu_f/k_f \quad (12)$$

where c_{pf} is specific heat of air.

By expressing Nu_{fp} as in Equation 13 [24], it is possible to find solid and gas phase heat transfer.

$$Nu_{fp}=h_{fp}d_p/k_f \quad (13)$$

where h_{fp} is solid and gas phase heat transfer, d_p is solid particle diameter, and k_f is air thermal conductivity.

In order to calculate the minimum fluidization velocity for solid particles, Ergun equation that is suitable for particles used in this study that are classified as Geldart B, have density 3210 kg/m^3, and have diameter in the range of 250-1190 μm, shown in Equation 14 was used [25].

$$\vec{g}\left(\rho_p-\rho_f\right)=\frac{1.75\rho_f u_{mf}^{\,2}}{d_p\alpha_f^{\,3}}+\frac{150\mu_f\left(1-\alpha_f\right)u_{mf}}{d_p^{\,2}\alpha_f^{\,3}} \quad (14)$$

where u_{mf} is minimum fluidization velocity and $\vec{g}$ gravitational acceleration.

RESULTS AND DISCUSSIONS

The quartz tube fluidized bed solid particle solar receiver described in Wang et al. (2016) [10] is used in this study to define performance improving operating conditions and design parameters. The model consists of vertical quartz tube of 0.034 m diameter and 0.5 m height as seen in Figure 1. The solar radiation with a radiation intensity of 450 kW/m^2 comes from the opening located between 0.1 and 0.2 m section of the tube. The air as heat transfer medium enters the bed from the bottom and exits from the top. The bottom 0.3 m part of the bed is allocated for the placement of silicon carbide (SiC) solid particles of 3210 kg/m^3 density.

The model selections in the ANSYS Fluent software for the simulations provided the proper definition of the problem physics. The radiative heat transfer model was activated for solar radiation absorption by solid particles. Since the flow was estimated to be laminar, the laminar model was selected. With the arrangements in the software, the specific heat and thermal conductivity of solid particles were changed with temperature and the solid particle viscosities were predicted by kinetic theory of granular flows. The pipe inlet and outlet boundary conditions are velocity inlet and pressure outlet, respectively. On the wall where solar radiation comes, the radiation intensity of 450 kW/m^2 was defined using the radiation boundary condition. In multiphase flow, the phasic momentum equations, the shared

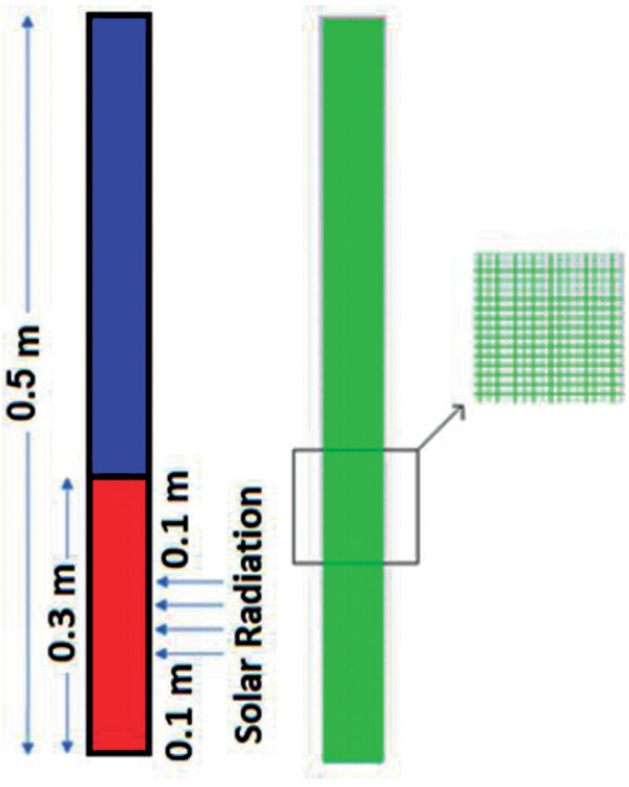

Figure 1. Study geometry and computational mesh.

pressure, and the phasic volume fraction equations are highly coupled.

There are several methods available in ANSYS Fluent code to treat this coupling. The Phase Coupled SIMPLE solves the velocities by coupling phases in a segregated fashion. This method has proven to be robust. The Coupled scheme simultaneously solves all equations for shared pressure and phase velocity corrections. This method works very efficiently in steady-state situations, or for transient problems when larger time steps are required. The Coupled with Volume Fractions option simultaneously couples the correction for volume fraction and velocity and shared pressure corrections. The method is advantageous for dilute situations. The Volume Fraction Coupling Method aims to achieve a faster steady-state solution compared to the segregated method of solving equations. It may not be a suitable option for transient applications due to the significant overhead in CPU time compared to the segregated method, unless it is run with a larger time step size [21]. As a result, "Phase Coupled Simple" was used for pressure-velocity coupling and "Pressure-Based Solver", which is one of the solver options provided in ANSYS Fluent software, was used as a solver. The pressure-based solver is suitable for incompressible flows and low Mach number flows. On the other hand, the other option, density-based solver is for the transonic and supersonic flows [26].

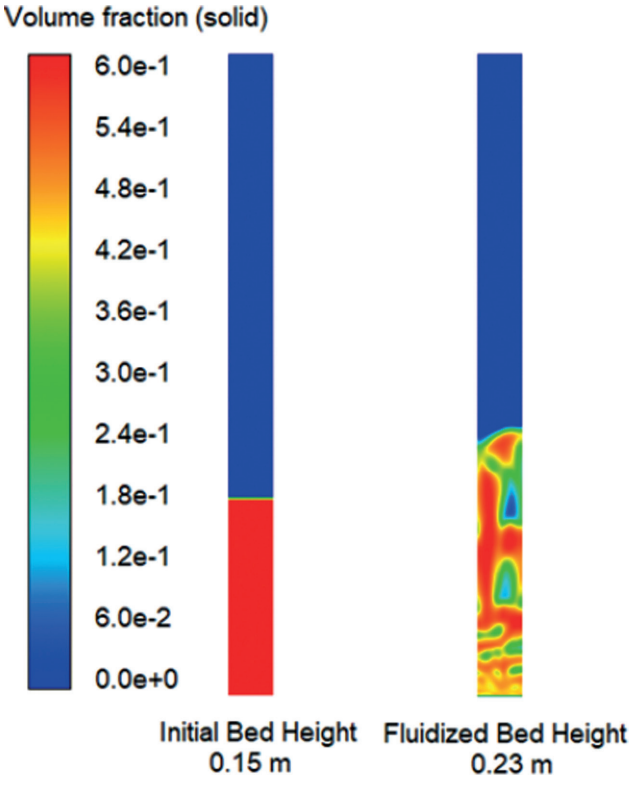

Figure 2. Verification of the CFD hydraulic model.

The grid independence study was carried out to make the results mesh independent. The results of this study indicated that 28035 nodes and 27200 elements in total is appropriate for this problem when comparison with 34710 nodes and 33782 elements and 6783 nodes and 7200 elements were performed which resulted 1.2% and 2.2% relative errors compared with the selected mesh, respectively. For time-dependent analyses, the time step size was taken as 0.001 s by considering Courant number.

The verification of the model choices and related parameters were performed by simulating the system with 500 μm diameter particles having 0.15 m bed height that is described as cold case in Wang et al. (2016) [10]. The experimental result of the bed expansion is given as 0.235 m. The simulation results in Figure 2 show the bed expansion is around 0.23 m which is compliant with the experimental data. The thermal model was also verified with experiment 3 of Zhang et al. (2015) [27]. The outlet temperature from the simulation was calculated as 701 K which is reported as 705.4 K in the experiment. This result shows the appropriateness of the thermal model.

Single Phase Flow Results

Before analyzing the two-phase flow hydrodynamics, the outlet temperature of single-phase case that no solid particles are added to the fluid was performed to create a reference result. The air with inlet velocity of 0.3 m/s enters the quartz tube from the bottom and exposed to solar radiation in the tube. It is seen in Figure 3 that the system comes to equilibrium in about 4 s and the maximum air outlet temperature obtained was determined as 421 K.

Figure 4(a) shows the equilibrium temperature distribution and Figure 4(b) shows the distribution of solar radiation in the system. As seen in Figure 4(a), the region where solar radiation enters the system has the highest temperature in the bed. The Figure 4(b) shows that the solar

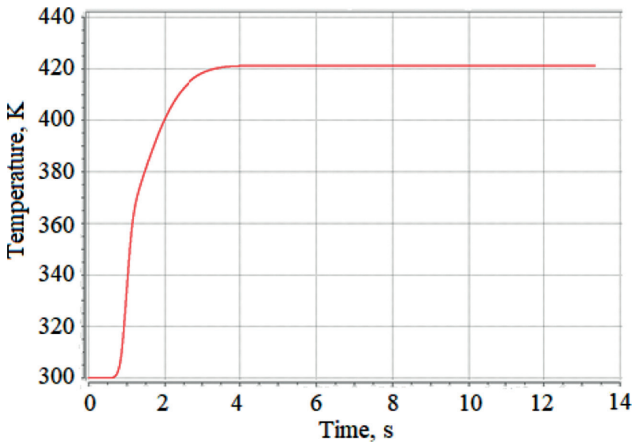

Figure 3. The variation of outlet temperature with time for single phase flow.

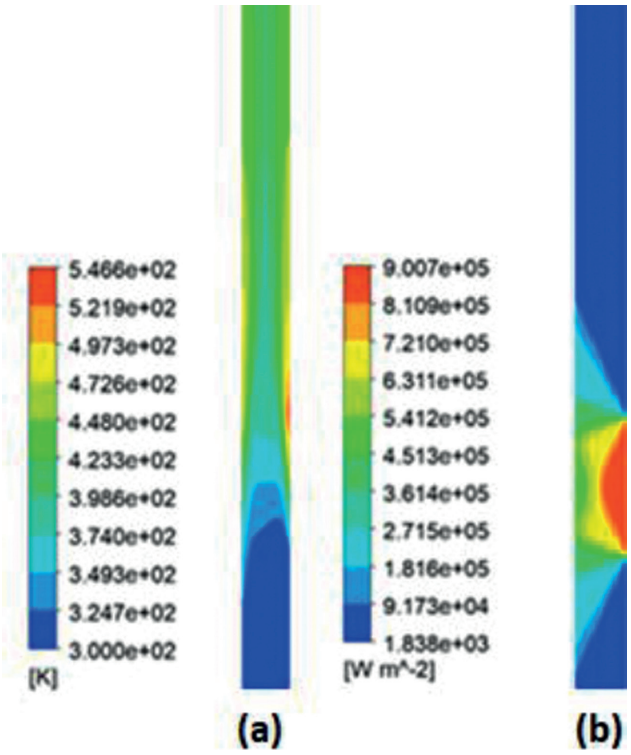

Figure 4. The distribution of (a) temperature (b) solar radiation in receiver for single phase flow.

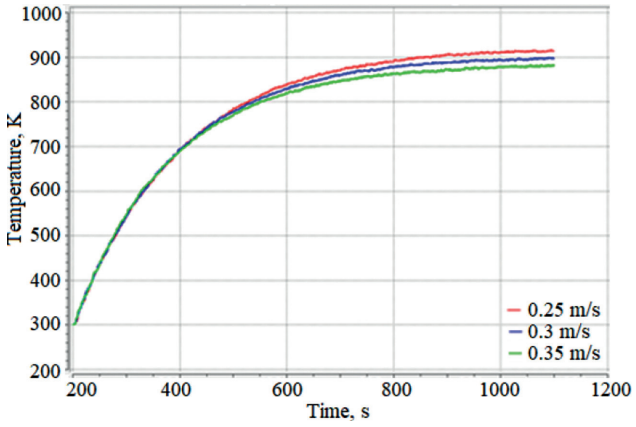

Figure 5. The variation of air outlet temperature with time for different inlet velocities.

radiation can reach the rearmost part of the pipe due to the high light transmittance of the air.

Multi-Phase Flow Results

Silicon carbide (SiC) particles which have high thermal conductivity and heat capacity were added to the system in order to increase the outlet temperature obtained from the system operating as single phase. The addition of solid particles must be performed carefully with consideration of the value of air inlet velocity, the number of particles in the

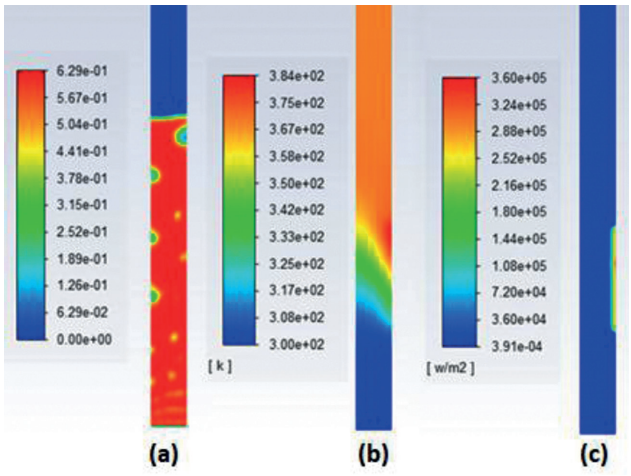

Figure 6. The distribution of (a) volume fraction of solids, (b) air temperature, (c) solar radiation in fixed bed.

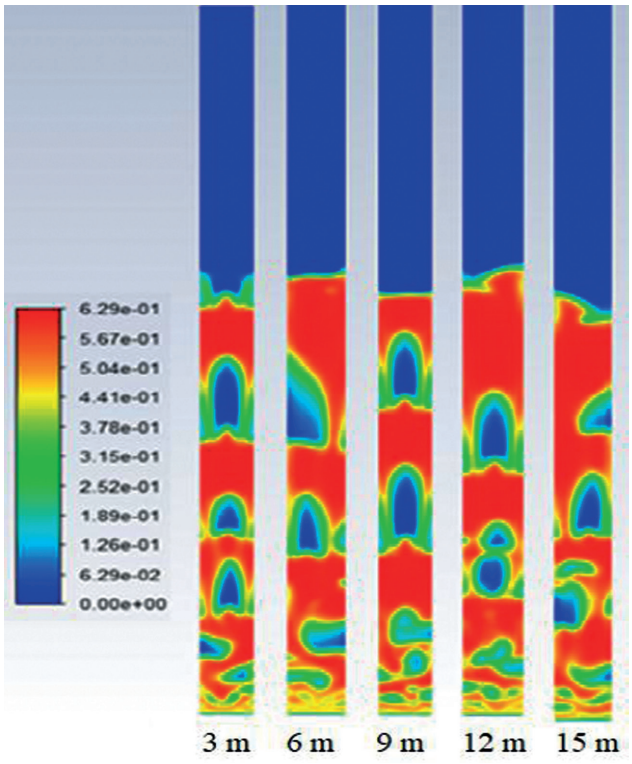

Figure 7. The variation of solid phase volume fraction in bed with time (v=0.25 m/s, d_p=400 μm, H=0.3 m).

bed, and particle size. The following sections examine these parameters to find their effect on bed thermal performance and hydrodynamics.

The effect of inlet velocity

SiC particles of 400 μm diameter were added to the system to create 0.3 m bed height. The minimum fluidization velocity for this case was calculated as 0.18 m/s by using

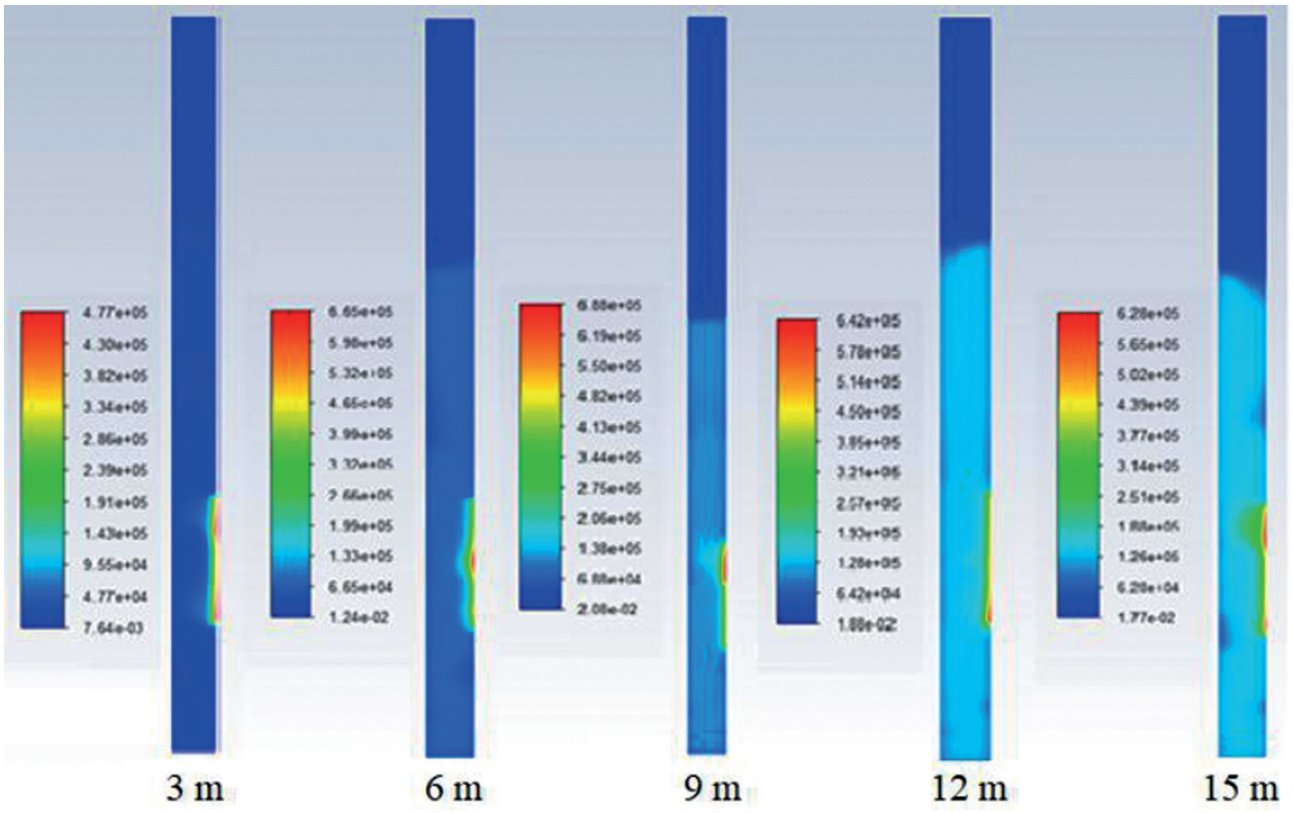

Figure 8. Variation of solar radiation distribution (W/m^2) in bed with time (v=0.25 m/s, d_p=400 μm, H=0.3 m).

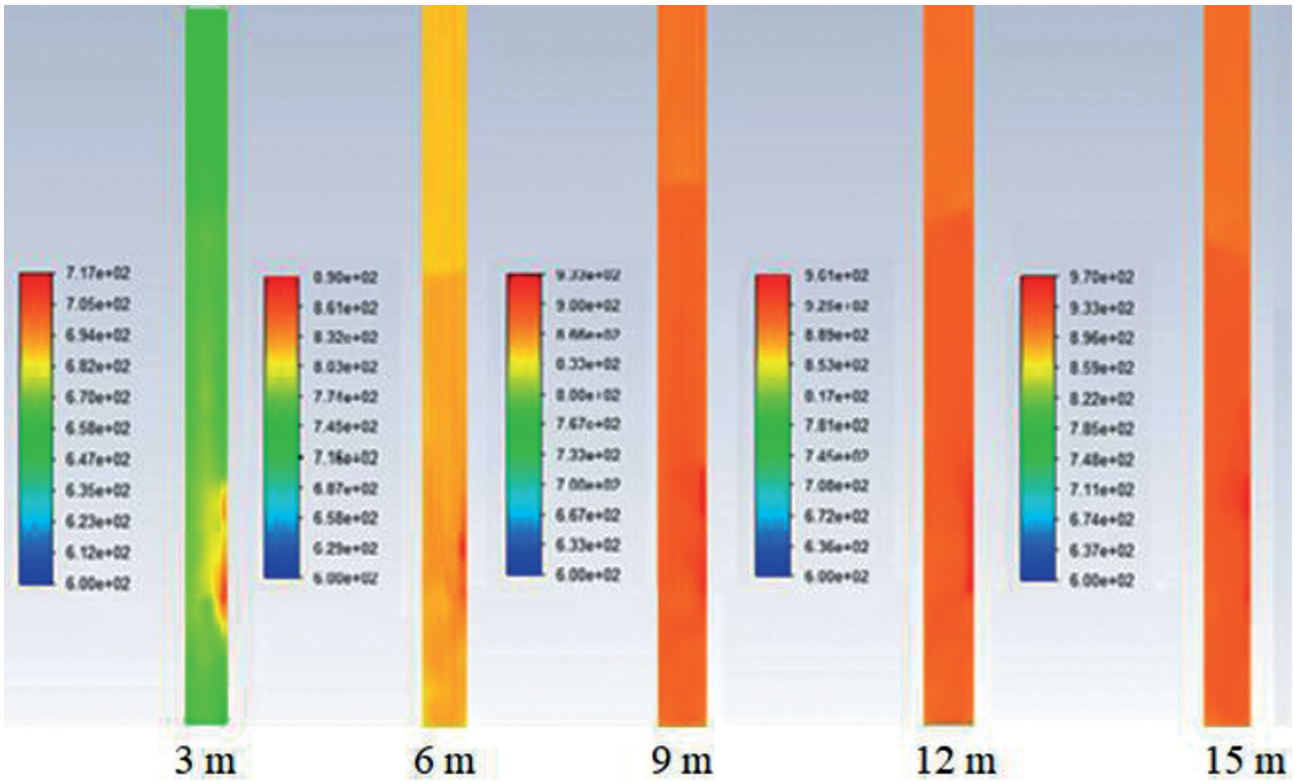

Figure 9. The variation of air temperature in bed with time (K) (v=0.25 m/s, d_p=400 μm, H=0.3 m).

Equation 14. The inlet velocity of air into the bed should be at least equal to this value for proper fluidization and should not be too big since it can cause pneumatic transfer of particles out of the bed. As a result, the air inlet velocities of 0.25, 0.3 and 0.35 m/s were selected. As can be seen from Figure 5, the outlet temperatures for 0.25, 0.3 and 0.35 m/s air inlet velocity cases are 913, 895 and 881 K, respectively indicating that increase in inlet velocity decreases the outlet temperature due to the fact that both the amount of solar radiation absorption of air and solids and the time for heat transfer between solid and air decreases. It is clear that these values are much higher than the value of 421 K for single phase case. The temperature increase is 116%, 112%, and 109%, respective to above inlet velocities. As mentioned above the air inlet velocity cannot be reduced indefinitely since fluidization retards with decrease in inlet velocity. In order to investigate this situation, a simulation for an air inlet velocity of 0.1 m/s, which is lower than the

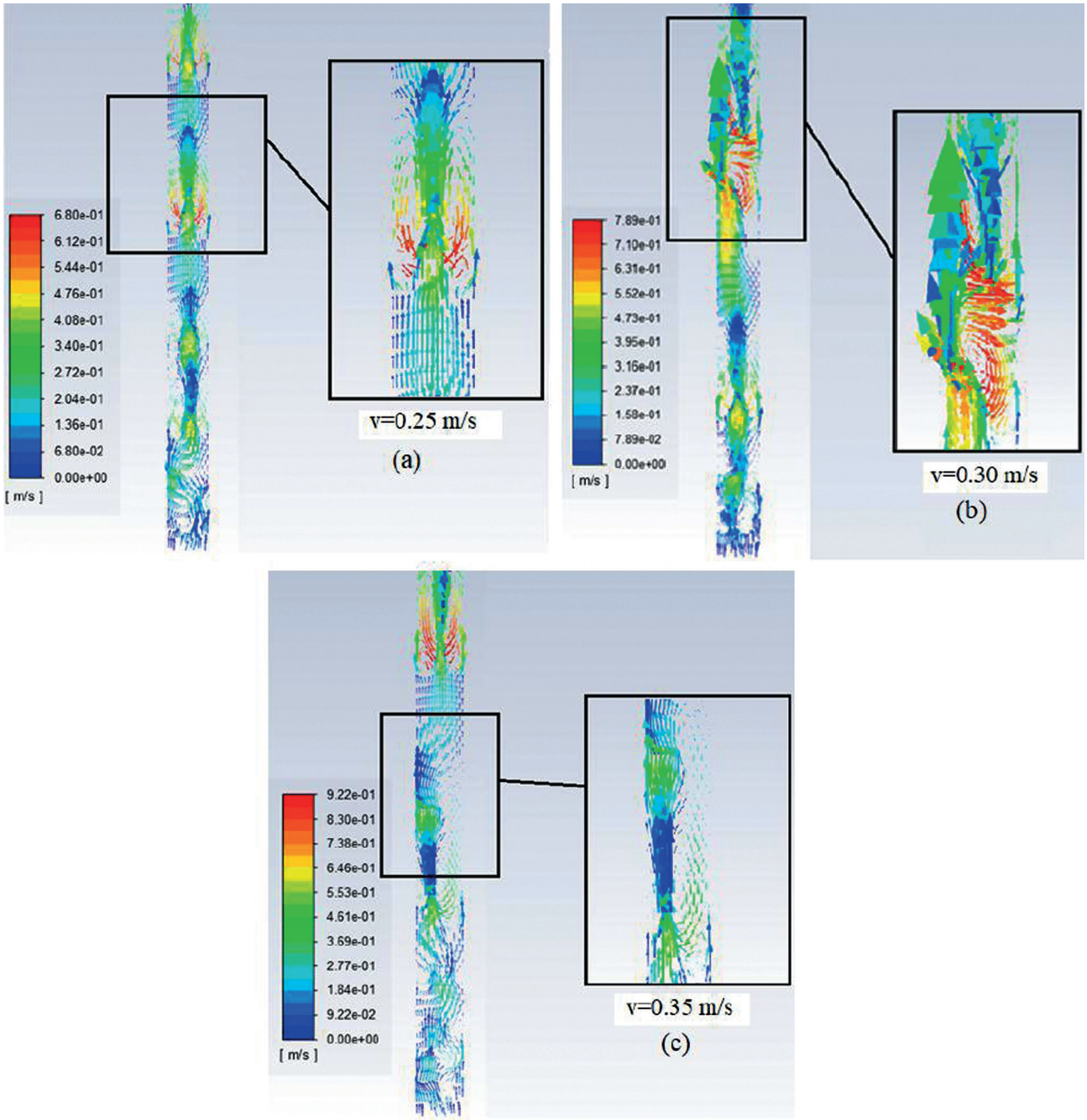

Figure 10. The velocity vector of solid phase (a) v=0.25 m/s, (b) v=0.30 m/s, (c) v=0.35 m/s (d_p=400 μm, H=0.3 m, t=3 m).

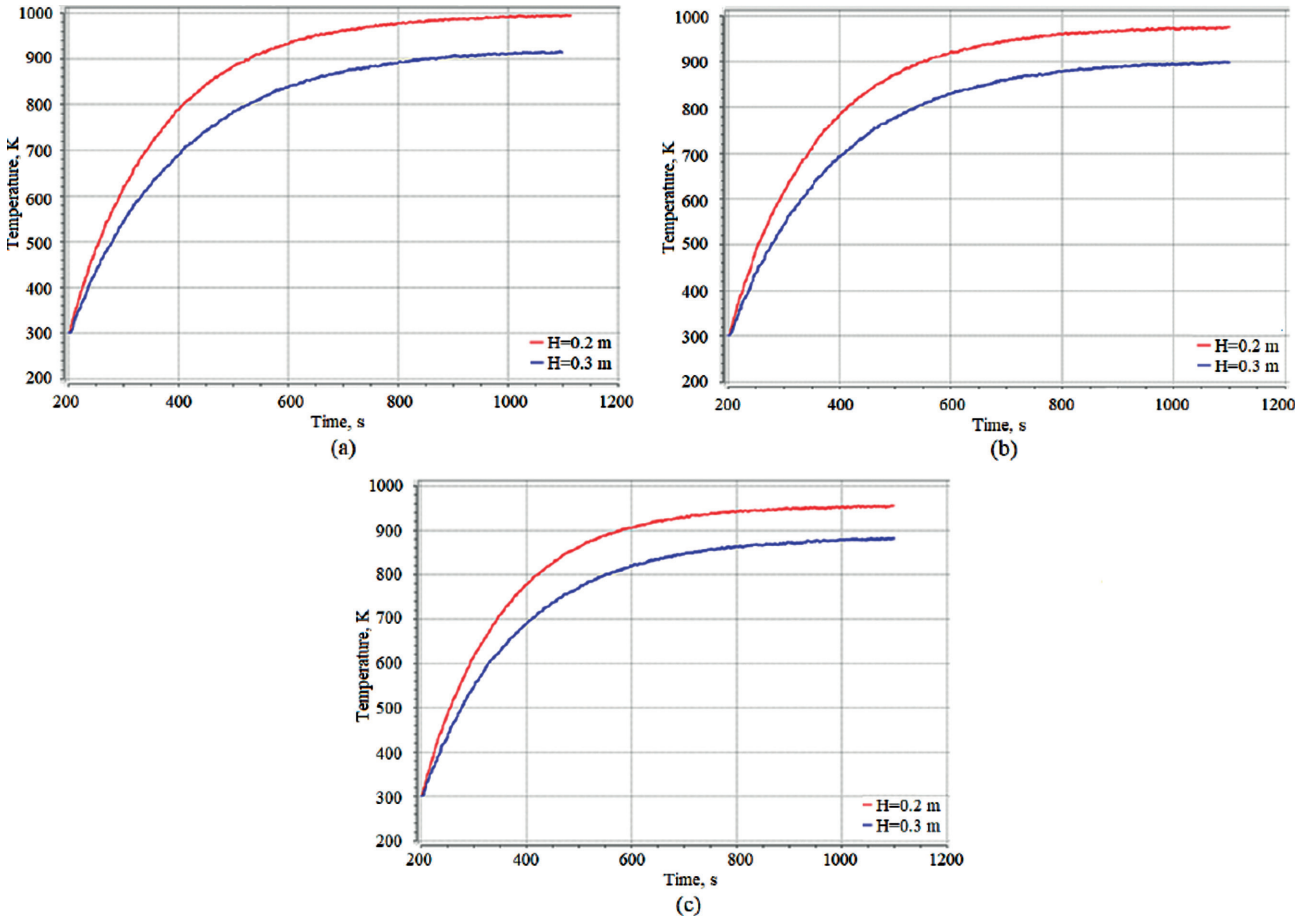

Figure 11. The effect of bed height on outlet temperature (a) v=0.25 m/s, (b) v=0.30 m/s, (c) v=0.35 m/s (d_p=400 μm).

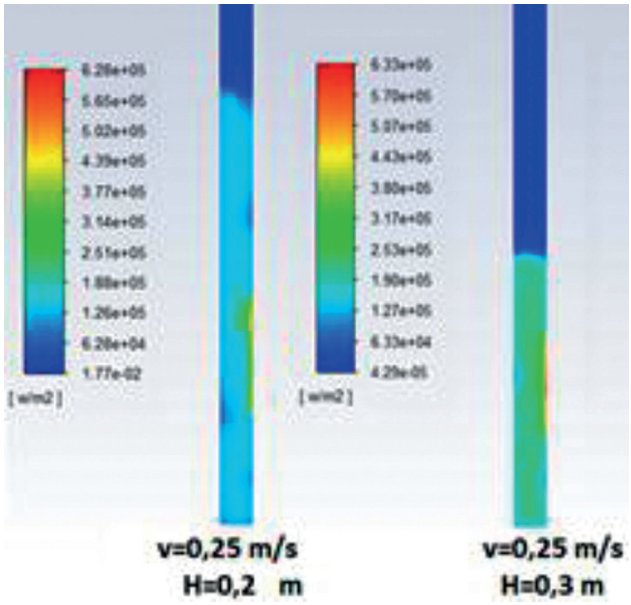

Figure 12. The variation of distribution of solar radiation with bed height (t=15 m).

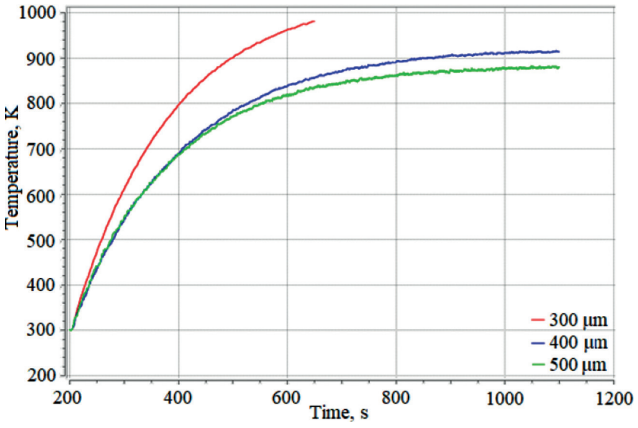

Figure 13. The effect of particle size on outlet temperature.

minimum fluidization velocity, was performed. As seen in Figure 6, the bed is fixed, no heating below the level of the opening for solar radiation, and no distribution of solar radiation in the bed. Although the outlet temperature is still higher than the single-phase case, it is way below than

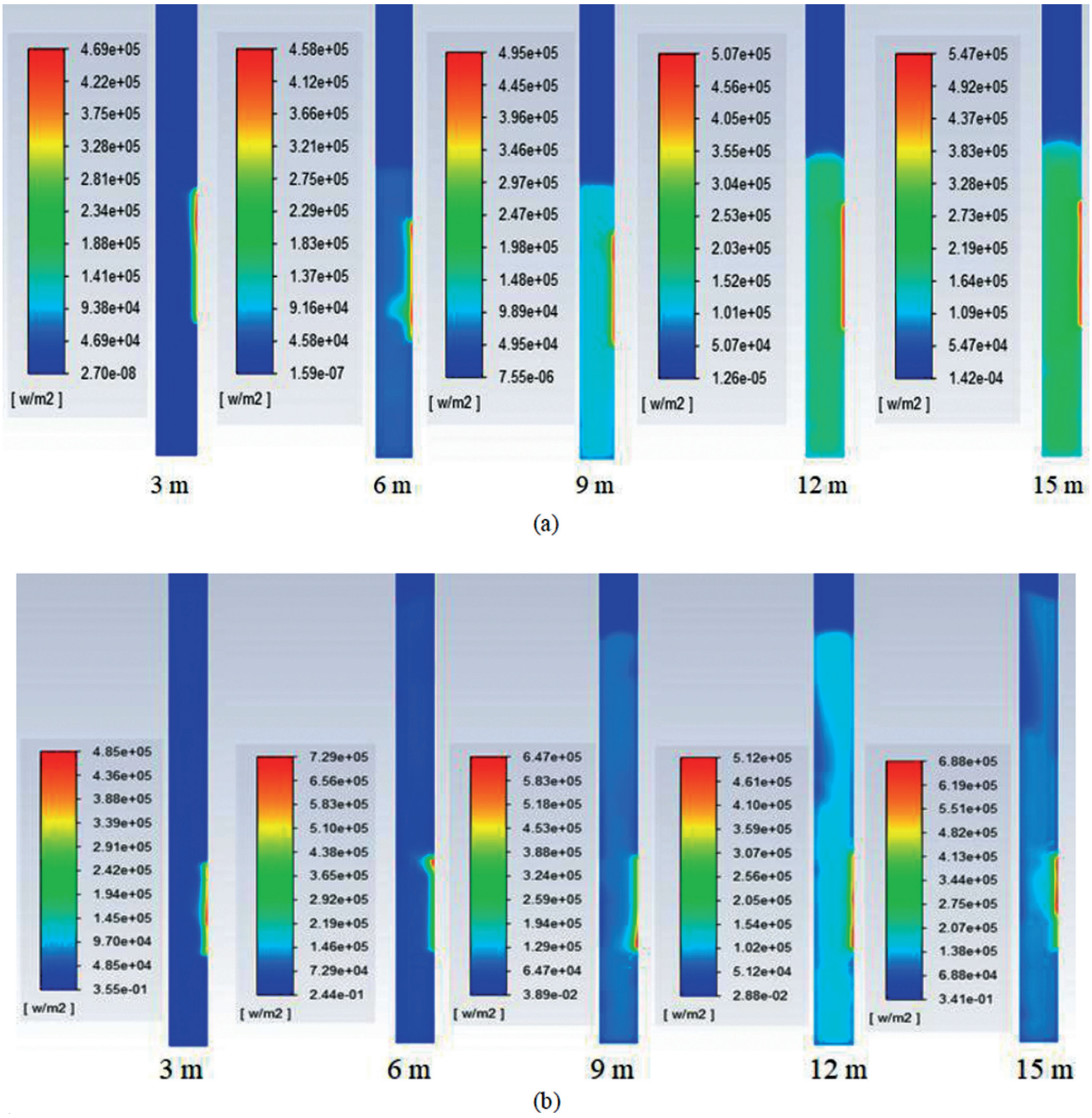

Figure 14. The distribution of solar radiation in the bed with time (a) for v=0.11 m/s, d_p=300 μm, (b) for v=0.36 m/s, d_p=500 μm. (H=0.3 m).

the fluidized bed cases since the solid particles block the incoming solar radiation and prevent the radiation from meeting with the solid particles and air at the opposite side of the opening.

The behavior of the distribution of temperature, radiation and solid phase volume fraction at different times during operation were also investigated. The data for inlet velocity of 0.25 m/s case are shown in Figures 7, 8 and 9. According to Figure 7, bubbling starts at the inlet of the bed immediately and at higher levels in the bed, bubbles coalesce and pushes the particles up in blocks. This flow is referred as "Slugging (Axial Slugs)" [24].

According to Figure 8, at the beginning of the heat transfer process, since the solar radiation absorption time in the system is short, the number of solid particles absorbing the radiation is low. However, it is observed that the spread of solar radiation increased later in the process. It should be noted that the amount of diffusion of

solar radiation may vary with the properties of the solid particle used in the system. The absorption and scattering coefficients of the particle directly affect the radiation absorption.

The distribution of the air temperature at different times in the system is shown in Figure 9. According to Figure 9, the temperature distribution in the system initially contains too much temperature difference. This situation coincides with the radiation distribution seen in Figure 8. In addition, the temperature increase is concentrated in the area that is directly exposed to solar radiation. However, as the system approaches equilibrium, the temperature difference in the receiver disappears.

To examine the flow hydrodynamics inside the solid particle fluidized bed receiver, the velocity vectors of the solid particles in the bed for 0.25, 0.30 and 0.35 m/s inlet velocity cases were plotted at 3 m of the operation time as seen in Figure 10. As can be seen from Figure 10, while the solid particles move upwards with fluidization in the bed, there are some local reverse flows. These reverse flows are usually on the sides of the upward moving slugs near the wall. This behavior indicates the solid particles in the system behaves as Geldart B particles and the slug flow.

The effect of bed height

The bed height was dropped to 0.2 m and the particle size and air inlet velocities were kept constant to perform comparison not only with single phase system but also with 0.3 m bed height case. Graphics showing the effect of bed height on outlet temperature are given in Figure 11. When the bed height is reduced to 0.2 m, the outlet temperatures at 0.25 m/s, 0.3 m/s, and 0.35 m/s change from 913 K to 994 K, 895 K to 974 K, and 881 K to 955 K, respectively. These values show that the addition of the solid particles to single phase system increases the system performance independent of the bed height.

The results in Figure 11 is subjected to discussion about why outlet temperature of air increases although a smaller number of solids are loaded into the bed when the bed height is reduced. This situation can be explained by using Figure 12.

According to Figure 12, when the bed height is 0.3 m, the upper 0.1 m part of the fluidized bed cannot be exposed to solar radiation. Therefore, the solid and gas phases heated by solar radiation in the lower regions transfer heat to these upper parts where the radiation cannot reach. This situation causes heat loss in the system. In order to better observe this conclusion, the heat losses in the system are examined for both bed heights and the results showed that heat losses are 22 K and 27 K for bed heights of 0.3 m and 0.2 m, respectively. Therefore, it is important to design tube opening both in terms of position and size carefully because this is the main factor that affects the operating condition of bed height.

The effect of particle size

The bed height was kept constant at 0.3 m and particles with 500 μm and 300 μm diameters were used to enlighten the effect of particle size on system performance. The minimum fluidization velocity was calculated for each case individually and the air inlet velocities were adjusted by using these values. Due to very long simulation time, 7.5 m of simulation was performed for 300 μm particle diameter case. The time variation of temperature in Figure 13 shows that 7.5 m simulation contains sufficient data to enable comparison.

As seen in Figure 13, the air outlet temperatures of the systems loaded with particles having 300 μm, 400 μm, and 500 μm diameters were found to be 980, 895 and 878 K, respectively. By reducing the particle diameter at constant bed height, more particles are loaded into the system as a result, both the absorption of solar radiation and the heat transfer surface increase. Figure 14 supports this conclusion by showing that the decrease in particle diameter causes better diffusion of solar radiation within the system. In addition, the inlet velocity of air drops since the minimum fluidization velocity decreases with particle size and as shown before this affects system performance positively.

CONCLUSIONS

The solid particle addition into a solar receiver in concentrated solar systems can increase the outlet temperature of the heat transfer fluid with direct or indirect exposure of these particles to concentrated solar radiation. In order to provide guidance on this addition, silicon carbide particles (SiC) were added into the quartz tube fluidized bed solar receiver with a 0.1 m opening for solar radiation entrance. Computational fluid dynamics simulations were performed to find optimum operating and design conditions.

The case without particle addition was performed first to identify the effect of adding particles into the system. The outlet air temperature of 421 K was achieved in this case. In fluidized bed systems, in order to have stable fluidization, the gas inlet velocity must be above the minimum fluidization velocity but below the pneumatic transfer velocity. It was observed from the simulations that the outlet temperature of the two-phase system is inversely proportional to the inlet air velocity since outlet temperatures of 913 K, 895 K, and 881 K were obtained for 400 μm diameter particles in 0.3 m bed for air inlet velocities of 0.25, 0.3, and 0.35 m/s. It is clear that solid particle addition to solar receivers increases the amount of heat transfer between the fluid and the solar radiation as well as between the fluid and solid particles. When compared with the single-phase system, maximum of 116% increase in outlet temperature was achieved with solid particle addition.

It is important to know how much solid particle is necessary to load into the fluidized bed since it affects the system performance. With 400 μm particle diameter and bed

height of 0.2 m, outlet temperatures of 994 K, 974 K, and 955 K were found. It was shown that the bed height being greater than the height of the opening where solar radiation comes reduces outlet temperature due to the fact that when the bed height is increased, the heat loss in the system increases because of heat transfer between the cold and hot parts of the bed. The increase in the outlet temperature is around 8% with bed height reduction. The maximum increase in outlet temperature was calculated as 136% when compared with the single-phase system.

Another important parameter for fluidized beds is the size of the particles that are loaded into the system. When particle diameters of 300 and 500 μm for bed height of 0.3 m was considered, outlet temperatures of 980 K and 878 K were calculated for respective minimum fluidization velocities. It was concluded that the outlet temperature of the system with small particles was higher since the number of particles loaded to the system increases for the same bed height. The reduction of particle size from 400 μm to 300 μm increases the outlet temperature 9.5%. On the other hand, increase of particle size from 400 μm to 500 μm decreases the outlet temperature only 2%. When compared with the single-phase system, maximum of 132% increase in outlet temperature was achieved with reduction of particle size.

In this study, the solar radiation intensity was assumed to be constant which is not the case in reality. Simulations with time varying solar radiation intensity can be done by using user defined function feature of the ANSYS Fluent code. The study is limited with the SiC particles because of the experimental setup. Other particle materials can be evaluated with the simulations. In addition, different insulation options can be studied.

NOMENCLATURE

α	Volume fraction
V	Volume, m^3
n	Number of phases
ρ	Density, $kg.m^{-3}$
$\vec{u}$	Velocity, $m.s^{-1}$
p	Pressure, $N.m^{-2}$
$\bar{\bar{\tau}}$	Reynolds stress tensor
$\vec{g}$	Gravitational acceleration, $m.s^{-2}$
$\vec{R}$	Interaction force between phases
h	Specific enthalpy, $J.kg^{-1}$
$\vec{q}$	Heat flux, $W.m^{-2}$
Q	Intensity of heat exchange between phases
I	Radiation intensity, $W.sr^{-1}$
$\vec{s}$	Direction vector
$\vec{s}'$	Scattering direction vector
$\vec{r}$	Position vector
α	Absorption coefficient
σ_s	Scattering coefficient
ϕ	Phase density
ω	Refractive index
T	Temperature, K
Ω'	Solid angle
Nu	Nusselt Number
Re	Reynolds number
Pr	Prandtl number
d	Particle diameter, m
μ	Dynamic viscosity, $kg.m^{-1}.s^{-1}$
c_p	Specific heat, $J.kg^{-1}.K^{-1}$
k	Thermal conductivity, $W.m^{-1}.K^{-1}$
h	Solid-gas heat transfer coefficient, $W.m^{-2}.K^{-1}$
t	Time, s

Subscripts

f	Fluid
p	Solid particle
mf	Minimum fluidization

AUTHORSHIP CONTRIBUTIONS

Mehmet Bölük: Methodology, Software, Validation, Formal analysis, Visualization.

Senem Şentürk Lüle: Conceptualization, Investigation, Resources, Supervision, Writing - Original, Draft, Writing - Review & Editing.

DATA AVAILABILITY STATEMENT

The authors confirm that the data that supports the findings of this study are available within the article. Raw data that support the finding of this study are available from the corresponding author, upon reasonable request.

CONFLICT OF INTEREST

The author declared no potential conflicts of interest with respect to the research, authorship, and/or publication of this article.

ETHICS

There are no ethical issues with the publication of this manuscript.

REFERENCES

[1] Kang Q, Dewil R, Degrève J, Baeyens J, Zhang H. Energy analysis of a particle suspension solar combined cycle power plant. Energy Convers Manag 2018;163:292–303. [CrossRef]

[2] Widyolar B, Jiang L, Ferry J, Winston R, Cygan D, Abbasi H. Experimental performance of a two-stage (50×) parabolic trough collector tested to 650 °C using a suspended particulate heat transfer fluid. Appl Energy 2019;240:436–445. [CrossRef]

[3] Ho CK, Christian JM, Yellowhair J, Armijo K, Nguyen C. Performance evaluation of a high-temperature falling particle receiver. 10th International Conference on Energy Sustainability collocated with the ASME 2016 Power Conference and the ASME 2016 14th International Conference on Fuel Cell Science, Engineering and Technology 2016.

[4] Kim JS, Kumar A, Gardner W, Lipiński W. Numerical and experimental investigation of a novel multi-stage falling particle receiver. AIP Conference 2019. [CrossRef]

[5] Ho CK. A review of high-temperature particle receivers for concentrating solar power. Appl Therm Eng 2016;109:958–969. [CrossRef]

[6] Al-Ansary H, El-Leathy A, Jeter S, Djajadiwinata E, Alaqel S, Golob M, et al. On-sun experiments on a particle heating receiver with red sand as the working medium. AIP Conference 2018. [CrossRef]

[7] Lopez PI, Benoit H, Gauthier D, Sans JL, Guillot E, Mazza G, Flamant G. On-sun operation of a 150 kWth pilot solar receiver using dense particle suspension as heat transfer fluid. Sol Energy 2016;137:463–476. [CrossRef]

[8] Benoit H, Perez Lopez I, Gauthier D, Sans JL, Flamant G. On-sun demonstration of a 750°C heat transfer fluid for concentrating solar systems: dense particle suspension in tube. Sol Energy 12015;18:622–633. [CrossRef]

[9] Johnson E, Baker D, Tari I. Proposal of a novel gravity-fed, particle-filled solar receiver. SOLARPACES 2016: International Conference on Concentrating Solar Power and Chemical Energy Systems 2016. [CrossRef]

[10] Wang F, Bai F, Wang T, Li Q, Wang Z. Experimental study of a single quartz tube solid particle air receiver. Sol Energy 2016;123:185–205. [CrossRef]

[11] Nie F, Cui Z, Bai F, Wang Z. Properties of solid particles as heat transfer fluid in a gravity driven moving bed solar receiver. Sol Energy Mater Sol Cells 2019;200:110007. [CrossRef]

[12] Kaijun J, Xiaoze D, Yanqian K, Chao X, Xing J. A comprehensive review on solid particle receivers of concentrated solar power. Renew Sust Energy Rev 2019;116:109463. [CrossRef]

[13] Segal A and Epstein M. The optics of the solar tower reflector. Sol Energy 2001;69:229–241. [CrossRef]

[14] Kodama T, Gokon N, Cho HS, Matsubara K, Etori T, Takeuchi A, et al. Particles fluidized bed receiver/reactor with a beam-down solar concentrating optics: 30-kWth performance test using a big sun-simulator. SOLARPACES 2015: International Conference on Concentrating Solar Power and Chemical Energy Systems 2016. [CrossRef]

[15] Kodama T, Gokon N, Cho HS, Matsubara K, Kaneko H, Senuma K, et al. Particles fluidized bed receiver/reactor tests with quartz sand particles using a 100-kWth beam-down solar concentrating system at Miyazaki. AIP Conference 2017. [CrossRef]

[16] Tregambi C, Padula S, Galbusieri M, Coppola G, Montagnaro F, Salatino P, et al. Directly irradiated fluidized bed reactor for thermochemical energy storage and solar fuels production. Powder Technol 2020;366:460–469. [CrossRef]

[17] Bellan S, Kodama T, Matsubara K, Gokon N, Cho HS, Inoue K. Heat transfer and particulate flow analysis of a 30 kW directly irradiated solar fluidized bed reactor for thermochemical cycling. Chem Eng Sci 2019;203:511–525. [CrossRef]

[18] Briongos JV, Gomez-Hernandez J, Gonzalez-Gomez PA, Serrano D. Two-phase heat transfer model of a beam-down gas-solid fluidized bed solar particle receiver. Sol Energy 2018;171:740–750. [CrossRef]

[19] Goldschmidt MJV, Beetstra R, Kuipers JA. Hydrodynamics modelling of dense gas-fluidised beds: comparison and validation of 3D discrete particle and continuum models. Powder Technol 2004;142:23–47. [CrossRef]

[20] Mahmood RA, Buttsworth D, Malpress R. Sharifian-Barforoush, A. CFD numerical and experimental investigation of two-phase flow development after an expansion device in a horizontal pipe. J Therm Eng 2021;7:307–323. [CrossRef]

[21] ANSYS Inc. ANSYS Fluent Theory Guide, Release 15.0., 2013;15:465–601.

[22] Gunn DJ. Transfer of heat or mass to particles in fixed and fluidized beds. Int J Heat Mass Transf 1978;21:467–476. [CrossRef]

[23] Parkash O, Kumar A, Sikarwar BS. CFD modeling of slurry pipeline at different prandtl numbers. J Therm Eng 2021;7:951–969. [CrossRef]

[24] Kunii D, Levenspiel O. Fluidization Engineering, 2nd ed. Newton: Butterworth-Heinemann; 1991.

[25] Anantharaman A, Cocco RA, Chew JW. Evaluation of correlations for minimum fluidization velocity (Umf) in gas-solid fluidization. Powder Technol 2018;323:454–485. [CrossRef]

[26] Mawali JA, Dakka SM. Numerical analysis of flame characteristics and stability for conical nozzle burner. J Therm Eng 2019;5:422–445. [CrossRef]

[27] Zhang Y, Bai1 F, Zhang X, Wang F, Wang Z. Experimental study of a single quartz tube solid particle air receiver. Energy Proced 2015;6:600–607. [CrossRef]